Journal of Environmental Management 301 (2022) 113872

Contents lists available at ScienceDirect

Journal of Environmental Management

journal homepage: www.elsevier.com/locate/jenvman

Performance evaluation of whey flux in dead-end and cross-flow modes via convolutional neural networks

Lukka Thuyavan Yogarathinam [a,b], Kirubakaran Velswamy [c], Arthanareeswaran Gangasalam [a,**], Ahmad Fauzi Ismail [b,*], Pei Sean Goh [b], Anantharaman Narayanan [a], Mohd Sohaimi Abdullah [b]

[a] Membrane Research Laboratory, Department of Chemical Engineering, National Institute of Technology, Tiruchirappalli, 620 015, India
[b] Advanced Membrane Technology Research Centre (AMTEC), Universiti Teknologi Malaysia, 81310, Skudai, Johor, Malaysia
[c] Department of Chemical and Materials Engineering, Donadeo Innovation Center for Engineering, University of Alberta-T6G 1H9, Edmonton, Canada

ARTICLE INFO

Keywords:
Convolutional neural networks
Filtration modes
Flux dynamics
Fouling
Whey

ABSTRACT

Effluent originating from cheese production puts pressure onto environment due to its high organic load. Therefore, the main objective of this work was to compare the influence of different process variables (trans-membrane pressure (TMP), Reynolds number and feed pH) on whey protein recovery from synthetic and industrial cheese whey using polyethersulfone (PES 30 kDa) membrane in dead-end and cross-flow modes. Analysis on the fouling mechanistic model indicates that cake layer formation is dominant as compared to other pore blocking phenomena evaluated. Among the input variables, pH of whey protein solution has the biggest influence towards membrane flux and protein rejection performances. At pH 4, electrostatic attraction experienced by whey protein molecules prompted a decline in flux. Cross-flow filtration system exhibited a whey rejection value of 0.97 with an average flux of 69.40 L/m^{2}h and at an experimental condition of 250 kPa and 8 for TMP and pH, respectively. The dynamic behavior of whey effluent flux was modeled using machine learning (ML) tool convolutional neural networks (CNN) and recursive one-step prediction scheme was utilized. Linear and non-linear correlation indicated that CNN model (R^2 – 0.99) correlated well with the dynamic flux experimental data. PES 30 kDa membrane displayed a total protein rejection coefficient of 0.96 with 55% of water recovery for the industrial cheese whey effluent. Overall, these filtration studies revealed that this dynamic whey flux data studies using the CNN modeling also has a wider scope as it can be applied in sensor tuning to monitor flux online by means of enhancing whey recovery efficiency.

1. Introduction

Dairy biorefineries have gradually processed cheese whey waste to produce valued added products which can be used in the production of biofuels and biochemicals. The dairy industry requires an enormous amount of water for the production of yogurt, cheese, butter etc. The discharge of dairy effluent causes water eutrophication and adverse effects towards the environment due to its high organic content (Asunis et al., 2020). Among the effluents produced by dairy industries, cheese whey effluent is observed to exhibit high biological oxygen demand (BOD) and chemical oxygen demand (COD) values (Charalambous and Vyrides, 2021; Fernández-Rodríguez et al., 2021). Cheese manufacturing factories discharge a greenish-yellow fluid called whey, which is a high value supplementary diet product. The effluent also constitutes of organic compounds, soluble proteins and other inorganic salts (Yadav et al., 2015). Therefore, it is necessary to fractionate these value-added whey proteins. In this regard, ultrafiltration (UF) is the preferred method for sustainable recovery of whey protein from cheese whey effluent (Das et al., 2016; Macedo et al., 2015). The fractionated nutrient-rich permeate can also be used as a substrate for microorganism in bioenergy generation (Luo et al., 2011). The superiority of UF is due to its high protein selectivity, high energy efficiency and ease of scale-up. However, the limitations of UF membrane include fouling and concentration polarization. Such factors lead to a reduction in flux performance and product recovery. To overcome this issue, membrane modification (Arunkumar and Etzel, 2015; Farjami et al., 2020;

* Corresponding author.
** Corresponding author.
E-mail addresses: arthanaree10@yahoo.com (A. Gangasalam), afauzi@utm.my (A.F. Ismail).

https://doi.org/10.1016/j.jenvman.2021.113872
Received 27 January 2021; Received in revised form 8 September 2021; Accepted 26 September 2021
Available online 1 October 2021

Vatanpour and Haghighat, 2019), tuning of experimental conditions (Hartinger et al., 2020), optimization of feed properties (Hartinger et al., 2020; Srivastava et al., 2021) and module configurations (Meyer et al., 2015) are the most viable alteration undertaken to control membrane fouling. Less emphasis has been placed on control of process variables.

Experimental modeling of process variable can be a convenient and cost-effective method to optimize the ultrafiltration of cheese whey effluent. Dead-end and cross-flow systems are the common modes of membrane filtration and control of feed flow pattern is an efficient method in restricting interaction between feed and membranes. Dead-end modules are commonly adopted for the concentration of low volume high value products (Zhang et al., 2019). Cross-flow configurations are preferred in large-scale applications for the recovery of value-added products such as proteins, polyphenols and bio-active compounds from wastewater (Biswas et al., 2021; Kekre et al., 2021; Li et al., 2020; Sánchez-Arévalo et al., 2021). Solute transport is a complex phenomenon in whey protein filtration, which depends on membrane characteristics and process variables such as transmembrane pressure (TMP), cross-flow velocity/angular velocity and feed properties (Adi et al., 2019; Corbatón-Báguena et al., 2018; Lee et al., 2017; Rezaei et al., 2011). Thus, flux prediction is an important tool to enhance filtration performance and understanding of fouling phenomenon. Resistance in series model is prevalently used in protein UF to estimate fouling and concentration polarization resistance. Other theoretical models such as concentration polarization and osmotic pressure models are also used to study protein flux and transport behavior in UF. However, it has a number of limitations as, (i) mathematical models are quite complex and requires more experiments to determine the intrinsic parameter of membranes. (ii) The assumption of models varies with respect to feed solution and (iii) models have poor correlation to predict the dynamic flux profile. To overcome these limitations, artificial intelligence (AI) is being deployed in various domains especially in the optimization of multivariate systems. Prevalent modeling tools such as artificial neural network (ANN) genetic algorithm (GA), fuzzy logic, least-square support vector machine (LSSVM) and hybrid modeling have also been utilized for membrane process optimization (Bagheri et al., 2019; Taheri et al., 2021). Recently, advanced AI tools like deep learning neural networks have been adopted in wastewater treatment to accurately predict the optimal operating conditions through multiplayer layered networks (Ma et al., 2020; Oulebsir et al., 2020; Park et al., 2019; Shi and Xu, 2018).

Convolutional neural network (CNN) is a type of deep learning neural network which convolutes the input data to obtain further moments and extract features from it. It is also capable of higher learning generalization. A powerful tool, it is preferred in a wide range of environmental management based applications such as flood risk management, automated waste composition estimation, air quality forecasting, visual pollutant classification, paper industry wastewater treatment, biodiesel wastewater reclamation and soil microplastic contamination analysis (Ahmed et al., 2019; Jialei Chen et al., 2021a; Junjie Chen et al., 2021b; Li et al., 2021; Ng et al., 2020; Poornapushpakala et al., 2021; Wang et al., 2020). Recently, CNN was adopted for the evaluation of membrane fouling in NF/RO and forward osmosis applications (Im et al., 2021; Park et al., 2019). Recursive single/multistep predictions have been utilized as simplified time series forecasting schemes. The main advantage of CNN over other neural network tool is that it is adaptation to local receptive fields to learn spatial hierarchy of input deep characteristics through its inherent structure of convolution, pooling, and fully connected layers. Another advantage is shared weights and biases which enhances the speed of data learning through reducing parameters (Kumar et al., 2021). CNN also enables translation invariant in the identification of global optimum. Hence, CNNs are often employed in time series prediction datasets for various domain applications (Wang et al., 2019). In a similar setup, CNN was deployed for flux dynamic prediction with respect to time in this study corresponding to multiple input variables (TMP, cross-flow velocity, angular velocity and pH of feed solution). To the best of our knowledge, studies on the development of CNN based model to predict the whey flux dynamics with respect to process variables is sparsely reported. A novel deep learning neural network based recursive one-step method was proposed to predict the whey flux. The main objectives of the study were (i) comparison of performance of polyethersulfone (PES) 30 kDa membrane in dead-end and cross-flow filtration system to recover whey protein from acid casein cheese whey solution (ii) analysis of the impact on sample efficiency for low volume dataset based modeling using CNN infrastructure (iii) the proficiency of membrane under optimum condition is assessed using industrial cheese whey effluent.

2. Experimental

2.1. Materials

Commercial PES 30 kDa membrane (M/s. Orelis environmental SAS, France) was used for whey protein UF in both cross-flow and dead-end filtration units. Chemicals such as hydrochloric acid (HCl), sodium carbonate, sodium-potassium, copper sulfate and Folin–Ciocalteu reagent were purchased from M/s. Merck India Limited. The chemicals used in the preparation and quantification of whey protein solution are of analytical grade. All the experiments were carried out using double distilled water. Milk was procured from a nearby milk processing industry.

2.2. Preparation of whey protein solution

The preparation procedure of acid casein cheese whey solution has been described in detail elsewhere (Pa'Ee et al., 2015). Initially, the milk was centrifuged at 6000 rpm for 15 min to remove fats and lipids. Subsequently, the pH of the milk solution was adjusted to 4.6 by adding 1 M HCl dropwise and the solution was left undisturbed for 20 min to allow casein precipitation. The solution after pH adjustment was then centrifuged at 6000 rpm for 15 min. Then, the feed solution was filtered with a piece of cheesecloth and thereafter the pH of the filtered solution was adjusted according to experimental conditions. The pH of the feed solution was maintained using 1 M NaOH. Repeated centrifugation of feed solution also contributed towards improvement in flux. The concentration range of total proteins in the feed solution was between 0.83 and 0.96 mg/ml. Feed solution was again centrifuged prior to filtration studies. The schematic of the preparation of acid whey protein solution is presented in Fig. S1.

2.3. Experimental design

The optimization of process variables has a significant influence in controlling solute-membrane interaction and thereby improves the filtration performance under energy efficient conditions. During filtration, the electrostatic interaction and shearing impact changes the configuration of protein moiety in response to manipulation of pH, TMP, and flow parameters (Miron et al., 2021). The effect of various process variables such as feed pH, TMP, cross-flow velocity, stirrer length and stirrer speed on the performance of whey protein filtration was evaluated. The influence of pH was studied by varying it between 4 and 8. The input experimental conditions, label and design of both dead-end (DE) and cross-flow (CF) filtrations are tabulated in Tables 1 and 2, respectively. In dead-end experiments, flow parameter conditions such as stirrer speed and stirrer length were varied at three different levels. Moreover, Reynolds number in stirred cell is a direct function of stirrer length (r) and stirrer speed (ω) (Becht et al., 2008). The stirrer length and stirrer speed were varied from 2 to 6 cm and 250–650 rpm, respectively. It is expressed as follows

$$\mathrm{Re}_{De} = \frac{\rho \omega r^2}{\mu} \tag{1}$$

Table 1
Experimental design, protein rejection coefficient data, fouling and concentration polarization resistance (%) of whey solution filtration in dead-end mode.

Exp. No	Test/ train	TMP (kPa)	Reynolds number	pH	Protein rejection coefficient	R_f ($x10^{12}$ m^{-1})	R_{cp} ($x10^{12}$ m^{-1})
DE1	Train	100	7.73×10^3	4	0.77	10.62	17.68
DE 2	Test	250	7.73×10^3	4	0.77	14.82	39.08
DE 3	Train	400	7.73×10^3	4	0.76	18.90	47.44
DE 4	Train	100	9.31×10^4	4	0.79	4.81	9.32
DE 5	Train	250	9.31×10^4	4	0.78	6.00	24.14
DE 6	Test	400	9.31×10^4	4	0.77	8.47	30.55
DE 7	Train	100	3.49×10^5	4	0.82	3.75	7.01
DE 8	Test	250	3.49×10^5	4	0.81	5.02	20.91
DE 9	Train	400	3.49×10^5	4	0.80	7.26	25.89
DE 10	Train	100	7.73×10^3	6	0.86	3.06	4.25
DE 11	Train	250	7.73×10^3	6	0.86	3.75	8.89
DE 12	Test	400	7.73×10^3	6	0.84	4.24	10.40
DE 13	Train	100	9.31×10^4	6	0.89	2.13	1.97
DE 14	Test	250	9.31×10^4	6	0.88	2.41	8.51
DE 15	Train	400	9.31×10^4	6	0.87	2.94	8.19
DE 16	Train	100	3.49×10^5	6	0.90	2.05	1.13
DE 17	Train	250	3.49×10^5	6	0.88	2.41	6.77
DE 18	Test	400	3.49×10^5	6	0.87	2.61	8.43
DE 19	Train	100	7.73×10^3	8	0.91	1.05	8.48
DE 20	Test	250	7.73×10^3	8	0.91	1.27	14.76
DE 21	Train	400	7.73×10^3	8	0.92	1.39	17.02
DE 22	Train	100	9.31×10^4	8	0.93	0.540	4.54
DE 23	Test	250	9.31×10^4	8	0.93	0.846	10.96
DE 24	Train	400	9.31×10^4	8	0.93	1.16	14.97
DE 25	Train	100	3.49×10^5	8	0.94	0.462	3.83
DE 26	Train	250	3.49×10^5	8	0.93	0.846	8.93
DE 27	Test	400	3.49×10^5	8	0.93	1.10	13.25

Table 2
Experimental design, protein rejection coefficient data, fouling and concentration polarization resistance (%) of whey solution filtration in cross-flow mode.

Exp. No	Test/ train	TMP (kPa)	Reynolds number	pH	Protein rejection coefficient	R_f ($x10^{12}$ m^{-1})	R_{cp} ($x10^{12}$ m^{-1})
CF1	Train	100	6.30×10^4	4	0.86	5.48	6.08
CF 2	Test	175	6.30×10^4	4	0.84	6.29	10.47
CF 3	Train	250	6.30×10^4	4	0.83	7.26	14.23
CF 4	Train	100	1.26×10^5	4	0.88	4.42	4.48
CF 5	Test	175	1.26×10^5	4	0.88	5.25	7.02
CF 6	Train	250	1.26×10^5	4	0.87	5.73	9.71
CF 7	Train	100	1.89×10^5	4	0.89	3.45	4.65
CF 8	Train	175	1.89×10^5	4	0.88	4.07	6.80
CF 9	Test	250	1.89×10^5	4	0.87	4.24	9.14
CF 10	Train	100	6.30×10^4	6	0.90	2.51	3.39
CF 11	Test	175	6.30×10^4	6	0.90	2.61	5.02
CF 12	Train	250	6.30×10^4	6	0.89	3.32	6.80
CF 13	Train	100	1.26×10^5	6	0.91	1.96	2.42
CF 14	Train	175	1.26×10^5	6	0.90	2.13	4.57
CF 15	Test	250	1.26×10^5	6	0.90	2.31	6.45
CF 16	Train	100	1.89×10^5	6	0.91	1.88	1.77
CF 17	Test	175	1.89×10^5	6	0.91	2.05	3.81
CF 18	Train	250	1.89×10^5	6	0.91	2.13	5.30
CF 19	Train	100	6.30×10^4	8	0.93	0.62	8.87
CF 20	Test	175	6.30×10^4	8	0.94	0.67	11.59
CF 21	Train	250	6.30×10^4	8	0.94	0.75	13.56
CF 22	Train	100	1.26×10^5	8	0.95	0.32	6.61
CF 23	Train	175	1.26×10^5	8	0.95	0.35	10.27
CF 24	Test	250	1.26×10^5	8	0.96	0.39	12.10
CF 25	Train	100	1.89×10^5	8	0.95	0.15	6.51
CF 26	Test	175	1.89×10^5	8	0.95	0.18	9.54
CF 27	Train	250	1.89×10^5	8	0.97	0.22	10.93

where $\rho$is the fluid density, ω is the angular velocity, $r$is the radius of stirred cell and $\mu$is the dynamic viscosity. The chosen operating range of cross-flow velocity was from 0.5 to 1.5 m/s, which was maintained by retentate control valve. The Reynolds number for tangential flow mode as a function of cross-flow velocity is given in Eq. (2).

$$\mathrm{Re}_{cf} = \frac{\rho u D_h}{\mu} \tag{2}$$

where $u$is the cross-flow velocity and D_h is the hydraulic diameter.

2.4. Experimental setup and protocol

Lab scale units of both cross-flow (Rayflow 100 Plate and Frame Mode) and dead-end ultrafiltration (Ultrafiltration cell-S76-400-Model, Spectrum USA) were used for filtration studies. The effective cross-sectional membrane area of both cross-flow and dead-end filtration units are 0.01 and 0.0038 m^2, respectively. Prior to experimental studies, a PES 30 kDa membrane was compacted using double distilled water in both filtration systems for 4 h under the higher level of constant TMP condition. Pure water flux (J_W) was measured by varying the TMP and was calculated using Eq. (3).

$$J_W = \frac{Q}{A} \tag{3}$$

where, Q is the permeate flow rate (m^3/s) and A is the effective cross-sectional area of the membrane (m^2). Permeability (L_w) is calculated

from the plot between TMP and pure water flux (J_W).

Prior to whey filtration, initial water permeability (L_{iw}) was measured using double distilled water. Then, whey solution was ultrafiltered for 120 min corresponding to experimental design. Again, the final water permeability (L_{aw}) was measured again to assess membrane fouling. Then, the membrane was cleaned with 0.2 wt% sodium dodecyl sulfate solution for 30 min. Finally, the membrane was washed using double distilled water and the permeability as measured again. Similar procedures were carried out for all filtration experiments. Fouling percentage was calculated using Eq. (4) given below.

$$Flux\ reduction\ ratio\ = \left(\frac{L_{iw} - L_{aw}}{L_{iw}}\right) \tag{4}$$

The protein concentrations in both permeate (C_p) and retentate (C_r) was quantified by Lowry's method (Metsämuuronen et al., 2011; Wen-qiong et al., 2017) and the total protein rejection coefficient was estimated using Eq. (5).

$$Protein\ retention\ coefficient\ = \left(1 - \frac{C_p}{C_r}\right) \tag{5}$$

The membrane performance index of individual input variables was dependent on whey flux, flux reduction ratio and protein retention coefficient. It was estimated as:

$$Membrane\ Performance\ Index = \left(\frac{Whey\ Flux \times Flux\ reduction\ ratio}{Protein\ retention\ coefficient}\right) \times 100 \tag{6}$$

Each experiment was performed twice and the reported values of flux, fouling percentage and total protein rejection percentage were obtained from the average of two experiments.

2.5. Fouling model

The two models used to assess the fouling behavior of whey solution are resistance in series and pore blocking models.

2.5.1. Resistance-in-series model

Resistance-in-series model is a physical model to evaluate the effect of input operating variables on fouling mechanism. Reversible fouling and irreversible fouling refers to the phenomenon of pore blocking either on the surface or within the interior pore structures and cake layer formation, respectively (Güneş and Gönder, 2021). The fundamental Darcy's law based resistance-in-series model relating to flux and TMP is expressed in Eq. (7).

$$J_w = \frac{\Delta P}{\eta\left(R_m + R_f + R_{cp}\right)} \tag{7}$$

where R_m, $R_f$and $R_{cp}$are resistance due to membrane, fouling and concentration polarization, respectively. It can be estimated using the following equations:

$$R_m = \frac{\Delta P}{\eta J_{wi}} = \frac{1}{\eta L_{iw}} \tag{8}$$

Irreversible membrane fouling is expressed as shown in Eq. (9)

$$R_f = \frac{\Delta P}{\eta J_{wf}} - R_m \tag{9}$$

Reversible membrane fouling is expressed as shown in Eq. (10)

$$R_{cp} = \frac{\Delta P - \sigma\Delta\pi}{\eta J_v} - R_m - R_f \tag{10}$$

where $J_{wi}$and J_{wf} are the initial and final water flux, respectively. $J_v$is cheese whey flux, $\sigma$is the reflection coefficient and $\Delta\pi$is osmotic pressure. Each experiment was performed twice and the reported values of flux and total protein retention coefficient were obtained from the average of the two experiments.

2.5.2. Pore blocking model

Hermia model is a mechanistic model employed to evaluate fouling based on membrane pore size and foulant size (Sundaran et al., 2019). The general expression of Hermia model for constant pressure dead-end filtration is represented as follows:

$$\frac{d^2t}{dV^2}(1+x)^n = k\left(\frac{dt}{dV}\right)^n \tag{11}$$

where t, V, k and n are the time of whey permeate (s), filtrate volume of whey solution (m^3), whey layer coefficients and empirical model constant, respectively. The value of n determines the type of fouling mechanism such as complete pore blocking (n = 2), standard pore blocking (n = 1.5), intermediate pore blocking (n = 1) and cake layer formation (n = 0). The expression of linear form of each models are described as follows:

The complete pore blocking is expressed as shown in Eq. (12)

$$\ln\left(J^{-1}\right) = \ln\left(J_0{}^{-1}\right) + k_{cb}t \tag{12}$$

The standard pore blocking is expressed as shown in Eq. (13)

$$\left(J^{-0.5}\right) = \left(J_0{}^{-0.5}\right) + k_{sb}t \tag{13}$$

The intermediate pore blocking is expressed as shown in Eq. (14)

$$\left(J^{-1}\right) = \left(J_0{}^{-1}\right) + k_{ib}t \tag{14}$$

The cake layer formation is expressed as shown in Eq. (15)

$$\left(J^{-2}\right) = \left(J_0{}^{-2}\right) + k_{cl}t \tag{15}$$

where J is the permeate flux of whey solution at a time t. J_0, k_{cb}, k_{sb}, $k_{ib}$and k_{cl} are pore blocking coefficients. The aforementioned models were adopted for the evaluation of both dead-end and cross-flow filtration. The individual pore blocking coefficients and coefficient of determination were obtained from the linear fit of whey flux data values.

2.6. CNN modeling

CNN process is based on the human brain's neural network, which involves the training of input datasets through neurons to achieve an optimum parameter solution. CNN model constitutes of three main structures, which are input layer, hidden layer and output layer. In CNN architecture, feature extraction and classification are basic components which are arranged hidden layer with multiple convolutional layer, pooling layer and classifiers. Fig. S2 shows the schematic structure of CNN. Moreover, the prime advantage of CNN is that the output data is also considered as an input data in means of identifying real time optimal solutions for higher ordered, complex applications. Thus, CNN is preferred in this study to model the whey flux dynamics with respect to time. In this study, the convolution layer was made of 32 mask with a kernel size of 3 × 3 and 2 × 2 for convolution and pooling layer, respectively. In CNN architecture, data of each input variables such as TMP, Reynolds number and feed pH were initialized by neuron connections through weighted input parameter such as weights (w_{ij}) and bias (b_i). The generalized representation of output function of neuron (y_i) to input and weighted input are expressed in Eq. (16).

$$y_i = \lambda\sum_{j=1}^{n} x_j.w_{ij} + b_i \tag{16}$$

where x_j and n are the input variables and number of input variables respectively. wij is the interconnected weight of i and j th neuron. λ is the activation factor. Activation function is a stimulating factor in

conversion of weighted inputs into output function for each neuron. Multi-Layer perceptron (MLP) feed forward neural network combined gradient descent algorithm was used for both training of datasets and convolutional layers. Rectified linear unit (ReLU) was used as an activation function in the hidden layer network. CNN model prediction of flux dynamics performance was evaluated using statistical parameter such as coefficient of determination (R^2), root mean square error (*RMSE*), and absolute average deviation (*AAD*) (Shanmugaprakash and Sivakumar, 2013). The statistical parameters were determined using the below equations:

$$R^2 = 1 - \frac{\sum_{k=1}^{n}\left(\widehat{y}_k - y_k\right)^2}{\sum_{k=1}^{n}(y_k)^2} \tag{17}$$

$$RMSE = \sqrt{\frac{1}{N}\sum_{k=1}^{n}\left(\widehat{y}_k - y_k\right)^2} \tag{18}$$

$$AAD = \left(\frac{1}{N}\sum_{k=1}^{n}\left(\frac{\left(\widehat{y}_k - y_k\right)}{y_k}\right)\right) \times 100 \tag{19}$$

where y_k and $\widehat{y_k}$ are the experimental flux and model predicted flux, respectively. *N* is the size of the dataset.

The modeling exercise was carried out on a computer powered by Intel CORE i3 CPU with 4 GB RAM running on Windows 10. The ML modules were implemented using Anaconda with built in Keras package which was utilized to train the networks using a version of the gradient descent algorithm. In the premise of this scheme, CNN on the other hand constituted of an input layer (4 neurons), one convolutional layer, a fully connected layer and an output layer (one neuron). The effect of fully connected layer was varied and studied on flux dynamic prediction. Flux data from the dead-end and cross-flow experiments were amplified using polynomial fit. In general, CNN requires large datasets to encounter over fitting and ensure accurate prediction. Then, the obtained 1592 polynomial fit experimental datasets of individual dead-end and cross-flow were subdivided randomly into training and testing. The training utilized 66% of original experimental data sets and the remaining 33% of was used to testing.

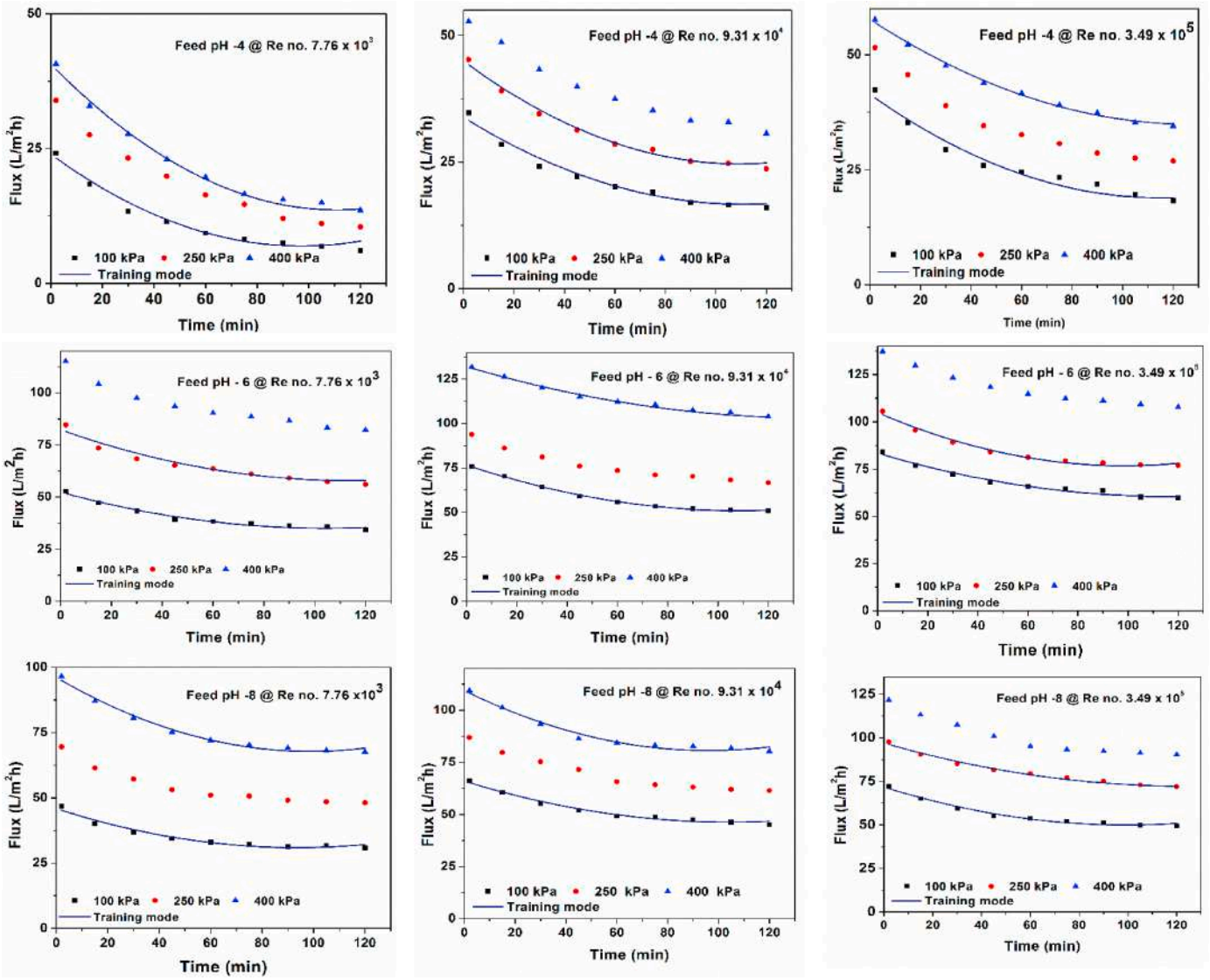

Fig. 1. Synthetic cheese whey flux pattern with respect to input variables and CNN training data of dead-end mode filtration.

3. Results and discussion

3.1. Evaluation of operating variables on cheese whey UF

The transport of whey solution across membrane relies on both diffusive and convective flow. Flux decline refers to a nonlinear behavior under constant pressure filtration as a function of time. Figs. 1 and 2 shows the synthetic whey flux pattern with respect to time for whey solution filtration in both dead-end and cross-flow modes, respectively. The desired threshold for cheese whey filtration was high protein retention ratio as well as flux with minimal fouling resistance. As seen in Figs. 1 and 2, the flux drop was rapid during the initial filtration period before attaining a pseudo steady state. Smaller ions present in the cheese solution adsorbs onto the membrane surface as well as pore walls, leading to an increment in transport resistance. Following that, a buildup of macromolecular protein on the membrane surface during filtration would lead to further flux decline. The regression analysis of membrane performance index as a function of input variables in dead-end and cross-flow mode of whey filtration are given as follows

$$Y\ (dead\ end) = -36.58 + 0.117\ TMP + 0.000057\ Reynolds\ No + 9.63\ pH$$

$$Y\ (cross\ flow) = -873.39 + 0.469\ TMP + 0.00223\ Reynolds\ No + 128.61\ pH$$

The desired significant factor in ANOVA analysis should be of higher Fishers statistical test F-value and lower p-value (<0.05). F-value is an indicator of statistical significance of a model, which is determined from the two mean squares of regression and residual error. The F-value for dead-end and cross-flow mode experiment are 13.36 and 16.74, respectively. The P-value was also less than 0.05 for all proposed input variables, which relies on the F-value and degree of freedom. From the ANOVA analysis, input variables such as TMP, stirrer speed, stirrer length, cross-flow velocity and feed pH are prime first order and have significant impact towards controlling the recovery of whey from cheese wastewater. Among the input variables, pH of the feed solution had the highest influence, valued at 75 and 87% in dead-end and cross-flow mode, respectively. In regards of the other input variables, TMP has a higher significance compared to Reynolds number. The regression model provided encouragement to analyze the effect of input variables on whey flux in both filtration modes. The fouling mechanism of whey solution on membrane with respect to input variables was evaluated using resistance in series (Tables 1 and 2) and pore blocking model

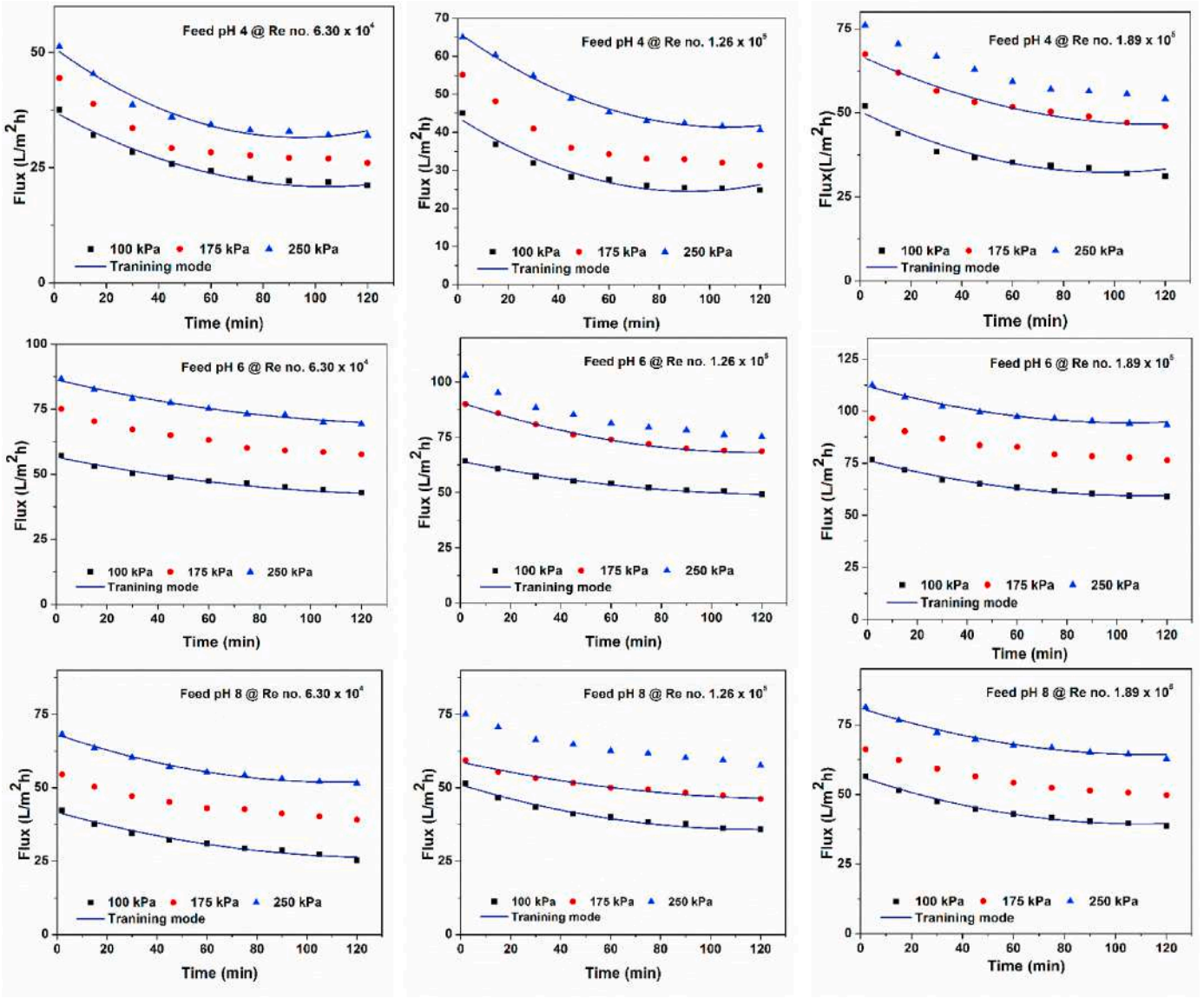

Fig. 2. Synthetic cheese whey flux pattern with respect to input variables and CNN training data of cross-flow mode filtration.

(Figs. S3 and S4, Tables 3 and 4) for both filtration modes, which are discussed in the following section.

3.1.1. Impact of pH on whey protein filtration

As seen in Fig. 1, the flux increased with an increase in pH from 4 to 6. The flux subsequently dropped when the pH reaches 8. In dead-end filtration mode, the highest and lowest average flux was observed at pH 6 (118.24 L/m^{2}h) (DE 18) and 4 (25.47 L/m^{2}h) (DE 1) respectively. This was due to the fact that protein transport through membrane relies on the isoelectric point of the feed solution. Isoelectric point refers to the net neutral charge point of protein. The isoelectric point of whey protein is reported to be 4.5 (Steinhauer et al., 2015). Proteins are negatively charge above isoelectric point and are positively charge when below it. Protein at isoelectric point weakens the electrostatic interaction and solubility property of whey solution. Acidic condition alter the electrostatic affinity between the amino acids of proteins that flows through the permeate. Hence, the experiments at pH 4 experienced a decrease in membrane flux values. It was mainly due to adsorption of whey proteins on the pores and pore walls of membrane. Fig. 3 shows the schematic of interaction between membrane and protein at different pH conditions. Flux results were in good correlation with fouling and concentration polarization resistance data were provided in Table 1. Fouling resistance data infer that fouling resistance decreased with an increase in pH value from 4 to 8 (Table 1). Higher fouling resistance (R_f) of 1.89×10^{13} m^{-1} was observed at a pH of 4 with lower Reynold number (DE 3). Tables 3 and 4 shows the pore blocking fouling coefficients of both dead-end and cross-flow experiments, respectively. The pore blocking plots for dead-end and cross-flow mode were provided in Figs. S3 and S4. As seen in Table 3, the R^2 values were higher and fit the cake layer model. The constant values of cake layer (K_{CL}) were higher for pH 4 as compared to 6 and 8. Higher cake layer constant of 4.32×10^7 s/m^2 was noticed at pH 4 together with a low TMP and Reynolds number (DE1). This indicates that the accumulation of whey protein hinders the movement of whey permeate. The K_{CL} value reduced to 9.99×10^5 s/m^2 in similar experimental condition at pH 8. Moreover, lower fouling resistance of 3.75 10^{13} m^{-1} was observed at a pH of 8 (DE 19). This phenomenon was because whey proteins were electrostatically bound onto the surface of membrane under acidic conditions (pH 4). This ultimately resulted in the decrease the protein rejection coefficient and lower protein rejection coefficient of 0.76 under a TMP of 400 kPa and lower Reynolds number (DE 3). Interestingly, a maximum protein retention coefficient of 0.94 was observed at pH 8 for dead-end filtration experiment mode (DE 25). This happened because proteins acquire higher negative charge and forms strong electrostatic repulsive force between them. This improves protein rejection coefficient and increases flux values (Valiño et al., 2014). The strong repulsive force led to the hindrance in solute transfer rate across the pores of the membranes. Thus, a minimal flux reduction ratio was observed in both filtration modes. At pH 6, the electrostatic interaction between whey proteins and membrane became weaker. At pH 6, the between whey proteins and membrane were weaker. Therefore, the electrostatic repulsive force aids in delivering higher flux values during filtration. Protein rejection coefficient increased significantly at pH 6 but the ratio was lower than of pH 8. This was because of the weaker surface charge interaction between proteins and membrane. The experimental flux analysis of both Hermia and the resistance and series model indicated that the pH of the feed solution has a substantial impact on both membrane flux and whey rejection performance. The filtration experiment analysis also assessed the adsorption of whey protein onto the surface and pores of membrane. Cheese whey batch adsorption with membranes was conducted for 16 h. However, the removal rate was minimal for all three pH values. The accumulation of protein was higher at pH 4 and it was also evident in surface topography analysis of adsorbed membrane surfaces. Fig. S5 shows the AFM topography of whey protein adsorbed membranes. A higher surface roughness value of 12.20 μm was observed for membrane subjected to adsorption at a pH of 4, whereas a lower surface roughness of 4.87 μm was observed at pH 8. This pH analysis depicted that stronger electrostatic repulsive force of proteins restricts the binding affinity between the feed solution and membrane. Hence, pH 6 and 8 was taken into consideration for evaluation of both TMP and flow variables.

3.1.2. Impact of TMP on whey protein filtration

TMP is a critical and major driving force in pressure driven membrane separation processes. From Figs. 1 and 2, it can be observed that

Table 3
Fouling mechanistic model (Pore blocking coefficients and statistical data) analysis of dead-end mode experiments.

Exp. No	Complete pore blocking		Standard pore blocking		Intermediate pore blocking		Cake layer	
	R^2	K_{CB} (s^{-1})	R^2	K_{SB} (m/s^2)	R^2	K_{IB} (m^{-1})	R^2	K_{CL} (s/m^2)
DE1	0.941	-1.85×10^{-4}	0.972	0.052	0.989	60.15	0.990	4.32×10^7
DE 2	0.968	-1.50×10^{-4}	0.986	0.034	0.995	30.67	0.987	1.31×10^7
DE 3	0.956	-1.54×10^{-4}	0.976	0.031	0.987	25.56	0.985	0.91×10^7
DE 4	0.951	-1.07×10^{-5}	0.971	0.0216	0.984	17.61	0.992	0.60×10^7
DE 5	0.943	-8.84×10^{-5}	0.961	0.015	0.975	10.20	0.991	0.24×10^7
DE 6	0.963	-7.48×10^{-4}	0.975	0.011	0.983	6.84	0.990	0.13×10^7
DE 7	0.944	-1.08×10^{-4}	0.966	0.019	0.980	14.76	0.983	0.42×10^7
DE 8	0.933	-9.06×10^{-5}	0.953	0.014	0.968	9.18	0.989	0.19×10^7
DE 9	0.969	-7.15×10^{-5}	0.98	0.010	0.988	5.95	0.997	0.11×10^7
DE 10	0.905	-5.56×10^{-5}	0.921	0.0082	0.934	4.84	0.959	8.52×10^5
DE 11	0.894	-4.79×10^{-5}	0.912	0.0055	0.928	2.55	0.954	2.75×10^5
DE 12	0.919	-4.24×10^{-5}	0.932	0.0041	0.943	1.60	0.961	1.22×10^5
DE 13	0.920	-5.80×10^{-5}	0.932	0.0071	0.943	3.47	0.961	4.20×10^5
DE 14	0.935	-4.60×10^{-5}	0.947	0.005	0.957	2.14	0.973	2.01×10^5
DE 15	0.958	-3.28×10^{-5}	0.964	0.0029	0.969	1.02	0.979	6.39×10^4
DE 16	0.854	-2.49×10^{-3}	0.949	0.0053	0.959	2.42	0.974	2.55×10^5
DE 17	0.854	-2.48×10^{-3}	0.867	0.0042	0.879	1.70	0.901	1.41×10^5
DE 18	0.918	-1.94×10^{-3}	0.927	0.0028	0.934	0.97	0.949	5.86×10^4
DE 19	0.867	-5.11×10^{-5}	0.887	0.008	0.906	5.02	0.939	9.99×10^5
DE 20	0.848	-4.72×10^{-5}	0.864	0.006	0.879	3.04	0.906	3.95×10^5
DE 21	0.861	-4.69×10^{-5}	0.875	0.005	0.888	2.15	0.911	1.99×10^5
DE 22	0.905	-5.06×10^{-5}	0.918	0.0066	0.931	3.42	0.953	4.65×10^5
DE 23	0.914	-4.86×10^{-5}	0.924	0.0055	0.932	2.46	0.947	2.51×10^5
DE 24	0.829	-4.01×10^{-5}	0.84	0.004	0.851	1.57	0.871	1.24×10^5
DE 25	0.872	-4.98×10^{-5}	0.887	0.0062	0.901	3.09	0.927	3.88×10^5
DE 26	0.942	-4.02×10^{-5}	0.952	0.0042	0.961	1.76	0.976	1.55×10^5
DE 27	0.890	-4.13×10^{-5}	0.899	0.0039	0.907	1.45	0.922	1.02×10^5

Table 4
Fouling mechanism model (Pore blocking coefficients and statistical data) analysis of cross-flow mode experiments.

Exp. No	Complete pore blocking		Standard pore blocking		Intermediate pore blocking		Cake layer	
	R^2	K_{CB} (s^{-1})	R^2	K_{SB} (m/s^2)	R^2	K_{IB} (m^{-1})	R^2	K_{CL} (s/m^2)
CF1	0.890	-7.57×10^{-5}	0.911	0.0138	0.929	10.148	0.958	2.78×10^{6}
CF 2	0.817	-6.92×10^{-5}	0.836	0.0115	0.854	7.64	0.886	1.72×10^{6}
CF 3	0.822	-6.21×10^{-5}	0.841	0.0094	0.859	5.77	0.892	1.09×10^{6}
CF 4	0.813	-7.52×10^{-5}	0.834	0.0127	0.862	8.60	0.902	2.01×10^{6}
CF 5	0.833	-7.47×10^{-5}	0.853	0.0112	0.873	6.78	0.907	1.26×10^{6}
CF 6	0.915	-6.80×10^{-5}	0.927	0.0091	0.937	4.90	0.955	7.17×10^{5}
CF 7	0.855	-6.20×10^{-5}	0.879	0.0094	0.902	5.78	0.940	1.10×10^{6}
CF 8	0.929	-5.03×10^{-5}	0.942	0.0065	0.954	3.33	0.978	4.44×10^{5}
CF 9	0.931	-4.67×10^{-5}	0.940	0.0056	0.949	2.67	0.963	3.08×10^{5}
CF 10	0.95	-3.69×10^{-5}	0.959	0.005	0.967	2.73	0.979	4.05×10^{5}
CF 11	0.946	-3.64×10^{-5}	0.953	0.0043	0.959	2.03	0.970	2.27×10^{5}
CF 12	0.966	-3.00×10^{-5}	0.971	0.0032	0.975	1.41	0.982	1.32×10^{5}
CF 13	0.943	-3.54×10^{-5}	0.951	0.0045	0.958	2.29	0.971	2.98×10^{5}
CF 14	0.932	-3.90×10^{-5}	0.940	0.0042	0.947	1.81	0.960	1.70×10^{5}
CF 15	0.913	-4.16×10^{-5}	0.924	0.0042	0.935	1.74	0.954	1.46×10^{5}
CF 16	0.925	-1.44×10^{-3}	0.920	0.0041	0.929	1.904	0.946	2.09×10^{5}
CF 17	0.925	-1.85×10^{-3}	0.933	0.0032	0.940	1.314	0.953	1.12×10^{5}
CF 18	0.890	-1.83×10^{-5}	0.898	0.0023	0.905	0.856	0.919	6.11×10^{4}
CF 19	0.959	-6.49×10^{-5}	0.97	0.0108	0.978	7.28	0.984	1.66×10^{6}
CF 20	0.940	-4.36×10^{-5}	0.951	0.0061	0.960	3.46	0.975	5.54×10^{5}
CF 21	0.917	-3.75×10^{-5}	0.926	0.0047	0.935	2.32	0.952	2.89×10^{5}
CF 22	0.931	-4.78×10^{-5}	0.939	0.007	0.951	4.11	0.970	7.14×10^{5}
CF 23	0.946	-3.20×10^{-5}	0.954	0.0042	0.961	2.22	0.974	3.11×10^{5}
CF 24	0.931	-3.38×10^{-5}	0.940	0.004	0.948	1.87	0.963	2.08×10^{5}
CF 25	0.922	-5.05×10^{-5}	0.935	0.0071	0.947	3.98	0.968	6.35×10^{5}
CF 26	0.947	-3.97×10^{-5}	0.954	0.005	0.961	2.53	0.973	3.24×10^{5}
CF 27	0.928	-3.36×10^{-5}	0.936	0.0038	0.945	1.71	0.960	1.76×10^{5}

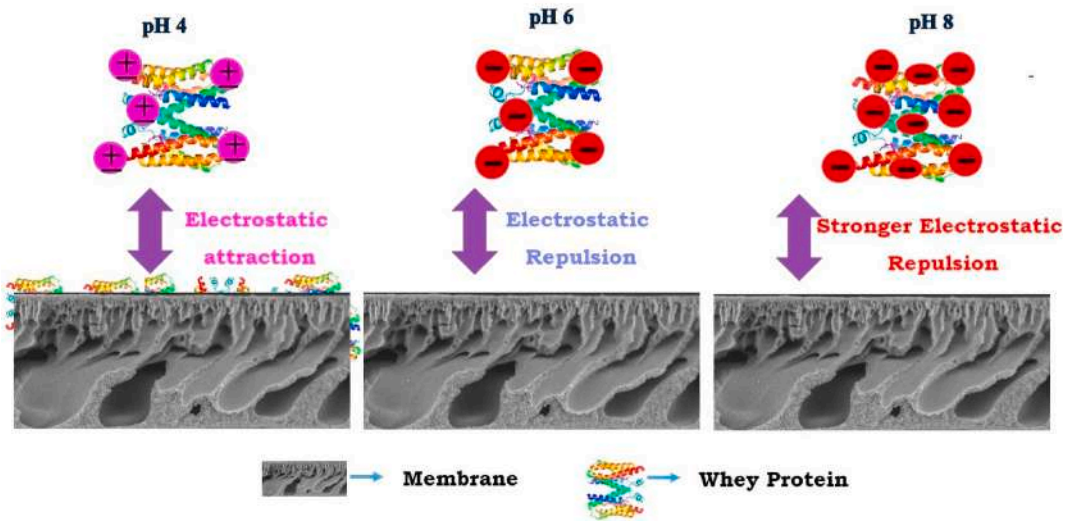

Fig. 3. Schematic of interaction between whey protein and membrane.

flux increases with the increase of TMP in both dead-end and cross-flow modes, respectively. This indicates that fluid flow resistance decreases with an increase of TMP and Reynolds number. At pH 6, a higher average flux of 118.24 and 99.44 L/m^2h was observed for dead-end and cross-flow filtration modes at a TMP of 400 and 250 kPa, respectively (DE 18 and CF 18). Higher flux is common due to convective transport mechanism. The results in this work are in good coherent with both fouling models. For instance, at pH 8 based experiments; the cake layer coefficient K_{CL} value was 9.99×10^5 s/m^2 in low TMP of 100 kPa (DE 19), which reduced to 1.99×10^5 s/m^2 for 400 kPa (DE21) (Table 3). This ensures that the permeate flow hindrance reduced with the increase of TMP. A similar observation was seen in other dead-end and cross-flow experiments corresponding to similar input variable conditions. However, it is imperative to note that the increase in TMP decreases protein rejection coefficient and increases fouling resistance. In both modes, fouling resistance increased with the increase of TMP from 100 to 400 kPa and 100–250 kPa (Tables 1 and 2). In both pH 6 and 8, a higher fouling resistance (R_f) of 4.24×10^{12} m^{-1} was observed in dead-end experiments at a TMP of 400 kPa and lower Reynolds number (7.76×10^3) (DE12). The resistance decreased at low TMP conditions (DE 10). This is owed to an increase in protein transport rate across the membrane at a TMP of 400 kPa. Such phenomena would eventually lead to the attachment of solute particles on the membrane surface pores, resulting in an increase in membrane fouling and decrease protein rejection coefficient (Jiang et al., 2018; Miller et al., 2014). Besides, concentration polarization resistance (R_{cp}) increased significantly with the increase of TMP. The centration polarization (R_{cp}) increased from 4.25×10^{12} m^{-1} to 1.04×10^{13} m^{-1} whenTMP increased from 100 to

400 kPa (DE10 to DE 12) (Table 1**)**. This was due to concentration polarization which is predominant under this phenomenon, since pore size of the membrane used is 30 kDa, which is smaller than whey protein. The molecular weight of whey proteins is within the range of 14 kDa–150 kDa. Thus, the concentration polarization resistance (R_{cp}) is higher than the fouling resistance (R_f) in all experiments. The Rcp was in good agreement with cake layer Hermia model analysis. The implication of different TMP was minimal towards protein rejection coefficient, which was due to the lower operating conditions range (100–400 kPa) (Tables 1 and 2). In cross-flow mode, flux increases progressively with the increase of TMP and Reynolds number (Fig. 2). Importantly, cake layer coefficient (K_{CL}), fouling (R_f) and concentration polarization resistance (R_{cp}) were lower as compared to dead-end experiments (Fig. S4).

3.1.3. Impact of flow parameters on whey protein filtration

In dead-end modes, the average flux exhibited increment with the increase of Reynolds number from 7.76×10^3 to 3.49×10^5. At pH 6 in high TMP conditions (Fig. 1), an average whey flux of 93.11 L/m^2h was observed for the Reynolds number of 7.76×10^3 (DE 12) and the flux increased up to a maximum of 118.24 L/m^2h at Reynolds number of 3.49×10^5 s/m^2 (DE 18). Comparatively, a similar trend in enhancement of flux was observed from 83.64 to 99.44 L/m^2h when the Reynolds number was increased in cross-flow mode experiments (Fig. 2). The enhancement of flux was minimal, which was due to the narrow range of operating conditions in cross-flow filtration modes. Similar observations were seen at pH 4 and 8. This was mainly due to the increase of stirrer speed, stirrer length and cross-flow velocity which promoted turbulence in the stirred cell and cross-flow module, respectively. This eventually resulted in the mitigating deposition of protein molecules on the membrane surface. This phenomena led to an increase in forced convection and back diffusive transport of solute from membrane solute to bulk (Verma and Sarkar, 2020). This was also evident in the resistance series analysis (Tables 1 and 2). and Hermia pore blocking model (Figs. S3 and S4, and Tables 3 and 4). A higher fouling resistance (R_f) of 1.83×10^{13} m^{-1} was observed for the lower Reynolds number of 7.76×10^3 at a cheese whey feed pH value of 4. However, it experienced reduction to7.26×10^{12} m^{-1} (DE 3) for Reynolds number of 3.49×10^5 (DE 9) at the same pH conditions. In cross-flow mode, fouling resistance (R_f) was maximum only up to 7.30×10^{12} m^{-1} for the Reynolds number of 6.30×10^4 (Table 2) (CF3). Similarly, an increase in Reynolds number reduces fouling and concentration polarization resistance. The cake layer coefficient (K_{CL}) also decreased from 1.22×10^5 to 5.86×10^4 s/m^2 when the Reynolds number in dead-end mode was increased from 7.76×10^3 to 3.49×10^5 at the experimental condition of pH 6 and 400 kPa (Table 3). Compared to dead-end mode, fouling resistance was remarkably lower and protein rejection coefficient also improved. This was due to the alteration of feed flow pattern in cross-flow mode. The flow pattern is parallel to the membrane surface in cross-flow modes. However, in dead-end mode, the flow pattern is perpendicular to the membrane surface. Perpendicular flow leads to adsorption of solute particles onto the membrane surface. In dead-end mode, initially, an increase in flux corresponded to an elevated TMP. Subsequently, accumulation of solutes on the membrane surface led to a reduction in flux. Flux has a linear relationship with the Reynolds number, which depicts that flow variables such as stirrer speed, stirrer length and cross-flow velocity have a significant influence on the flux performance of membrane. Both resistance in series model and pore blocking model indicated that the cake layer fouling mechanism is dominant. The theoretical models also had an advantage of significance on input variables for fouling mechanism. This observation would help to develop an effective way to control whey fouling in different filtration modes through optimization of hydrodynamic conditions.

3.2. Modeling with CNN

The experimental studies depicted that flux varies with respect to individual input variables and also exhibited a complex non-linear behavior with respect to time. This is unfavorable in industrial applications upon downstream processing. CNN was used as a modeling tool to predict the flux pattern with respect to various input variables. In general, humongous datasets available in other fields have enabled the employment of ML to find solutions for industrial issues. The versatility of datasets is expected to alleviate the biases and promote generalization of the learnt solutions. The disadvantage of utilizing ML schemes on datasets is that it has a very limited number of observations and also the possibility of over fitting. Hence, the frugality of the solution plays a major role in the eventual success of such applications. Adequate model development is essential to predict the precise process conditions appropriate for cheese whey filtration. Hence, the effects of algorithm, sample efficiency and epoch training on prediction of flux dynamics are discussed below.

Fig. 4a shows the algorithm effect on prediction of whey flux dynamics data of dead-end and cross-flow mode. As seen in Fig. 4**.**(a), adaptive moment estimation (adam), root mean square propagation (RMSProp) and nesterov-accelerated momentum (Nadam) optimizer displayed higher coefficient of determination (R^2) within the range of 0.9–0.94 for both modes. Among the optimizers, adam optimization algorithm showed desirable R^2 and RSME value, which was an extended version of the gradient descent optimization algorithm. Adam optimization algorithm is a combination of RMSProp and adaptive gradient (adagrad), which involves in the prediction of non-linear and sparse datasets. The improved flux prediction was due to the method used as it attains a good optimum solution through repeated convergence of weights (Yadav and Anubhav, 2020). Adaptive learning rate is another advantage in improving flux prediction. The adam gradient descent algorithm was adopted for further neuron and epoch optimization. Sample efficiency is an important metric in ML as it affects learning efficiency. A definition of sample efficiency would be the ratio between the number of samples and the number of trainable parameters for a given network to perform satisfactorily. In general, larger datasets are required in ML to accurately predict output responses. Optimum neuron and algorithm used has significant influences in controlling the structure of CNN when predicting flux. The number of neurons in the hidden layer is characterized by the dynamic flux data distribution with respect to time on corresponding input variables. The selection of neuron determines the overfitting and underfitting of flux datasets prediction, which make the model inefficient (Cavalcanti et al., 2019; Farahbakhsh et al., 2019). Fig. 4b shows the effect of trainable parameters on the prediction of flux dynamic data sets of dead-end and cross-flow modes. From Fig. 4b, the increase of training parameter showed better prediction with flux data dynamic data. It indicates that the increase in neuron layer improved prediction efficiency for optimum solution. The increase in training parameters enhances learning and momentum rate of datasets in CNN architecture. It eventually leads to error reduction in dataset training. The optimum neuron was determined to be at 60 and 50 for the dead-end and cross-flow modes, respectively. In this instance, CNN has specific features of identifying the global optimum in dataset through filters and hyper parameters (kernel size, stride and padding) (Cheng et al., 2021; Singh et al., 2021). The training parameters for dead-end and cross-flow mode are 377 and 317, respectively. Fig. 4**c** shows the epoch effect on prediction of flux dynamic data sets of dead-end and cross-flow mode. From Fig. 4**c**, optimal epochs were 90 for both dead-end and cross-flow modes. The R^2 value is 0.999 for both modes, which suggest that the epoch based training schemes in CNN was able to make better prediction on the whey flux data. This was due to the increase in the change of weights in neuron architecture. Furthermore, over fitting was observed with the enhancement of hyper parameters.

Figs S6(a-b) and **S6(**c-d) shows the CNN predicted test and train data whey flux dynamics data of dead end and cross flow mode, respectively.

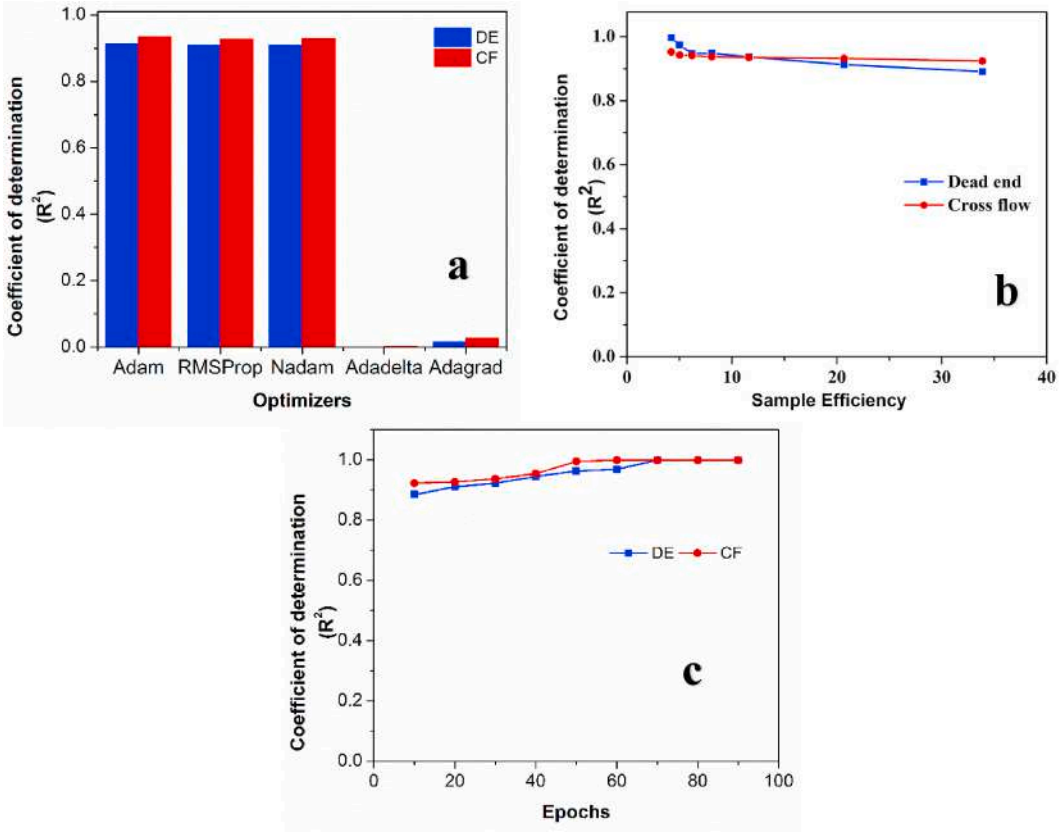

Fig. 4. (a–c) Impact of algorithm, sample efficiency and epochs on prediction of flux dynamics in dead-end (DE) and cross-flow (CF) mode.

From Fig. S6, CNN model predicted data fitted well with both training and testing experimental flux datasets for both cross-flow and dead-end modes. Table 5 shows the R^2, RMSE and absolute average deviation values of CNN predicted model for both cross-flow and dead-end mode. The R^2 value of the CNN predicted model for both cross-flow and dead-end mode are close to unity. Additionally, the values of other statistical parameter such as RSME and AAD values were coherent with CNN predicted model. The deviation of flux data in CNN was also lower than 5%. Linear and non-linear correlations were also evaluated to measure the CNN prediction, which is shown in Table 5. Linear correlation methods like Pearson correlation (Yaqub et al., 2020), Kendall correlation and nonlinear Spearman rank correlation (Arhoun et al., 2019) can be utilized for non-parametric measure of rank correlation between experimental and predicted flux data. The coefficients values from the data attained indicates a linear (Pearson and Kendall) and monotonic rank-based relationship (Spearman). Pearson correlation displayed a maximum value of 0.990 for dead-end mode. Between the modes, dead-end mode flux datasets exhibited higher correlation for Kendall and Spearman correlation. Though the values (between −1 and 1) indicate a reverse or direct dependency respectively between variables, they are not an accurate measurement of the relationship. This correlation analysis clearly depicts that deep learning CNN is a better model with superior accuracy in predicting flux dynamics in both filtration modes. The CNN model was also superior in predicting flux with frugal number of datasets through its optimized network. Table 6 shows the comparison of CNN predicted model flux dynamics with other membrane applications found in literature. As seen in Table 6, the CNN predicted model for whey flux dynamics results exhibited satisfactory R^2 with minimal datasets of training (66%). Moreover, other studies were conducted using dilute solutions and involving steady state modeling. It is therefore inferred from the metrics that CNN can be a suitable membrane modeling technique to predict membrane performance since it can work efficiently while utilizing a low number of dataset experiments. It would aid in the assessment of membrane modules in industrial operation to instruct of periodic washing and achieve higher flux values.

Table 5
Comparison of flux prediction parameters of CNN model.

Parameters	Dead-end mode	Cross-flow mode
	CNN	CNN
Coefficient of determination (R^2)	0.999	0.999
Root mean square error (RMSE)	0.231	0.292
Absolute average deviation (AAD)	0.007	0.122
Pearson	0.990	0.942
Kendall	0.910	0.822
Spearman	0.988	0.955

3.3. Industrial cheese whey solution

From the above experimental studies, cross flow system at the higher pH (8), TMP (250 kPa) and cross flow velocity (1.5 m/s) are found to be the optimum conditions for cheese whey filtration. These conditions were adopted to analyze real time industrial cheese whey effluent filtration studies. The characteristic of industrial cheese whey effluent was reported in our earlier research studies (Yogarathinam et al., 2018). Fig. 5 shows the industrial cheese whey flux of membrane with respect to time. As seen in Fig. 5, the flux experienced a slight decline with an increase of time whist rejection coefficient values remain constant. It was due to the attachment of cheese whey constituents on the membrane surface. The average flux and protein rejection coefficient of cheese whey effluent are 22.31 L/m^2h and 0.96, respectively. Both values were consistent for two different filtration cycles. Higher protein rejection coefficient can aid in reduction of organic load in the wastewater system. The flux was lower for real time industrial cheese whey effluent compared to synthetic whey solution simply because the former has a

Table 6
Comparison of prediction parameter with literatures.

S. No	Membrane system and feed solution	Output variables	Optimum flux (L/m^{2}h)	Model	Prediction accuracy (R^2)	References
1	Dead-end and oily wastewater	flux dynamics	19.30	ANN	0.987	Nandi et al. (2010)
2	Cross-flow and oil-wastewater	flux	216	ANN-genetic algorithm	0.999	Soleimani et al. (2013)
3	Cross-flow and red plum juice	flux dynamics	~8	ANN	0.961	Nourbakhsh et al. (2014)
4	Dead-end and surfactant wastewater	flux	5.6	Gene expression	0.989	Shishegaran et al. (2020)
5	Cross-flow and whey protein concentrate UF	flux dynamics	~110	Multiple regression analysis	0.999	María-José Corbatón-Báguena, Silvia Álvarez-Blanco (2018)
6	Spinning basket (5 kDa) and tea industry wastewater	flux dynamics	~41	ANN	0.9952	Saha et al. (2019)
7	Cross-flow forward osmosis and desalination	flux	–	ANN	0.931	Jawad et al. (2020)
8	Cross-flow forward osmosis and university effluent	fouling	–	CNN	0.90	Im et al. (2021)
9	Cross-flow and palm oil wastewater	flux dynamics	25.40	ANN	1.00	Yogarathinam et al. (2022)
10	Cross-flow and synthetic cheese whey	flux dynamics	69.40	CNN	0.999	Present study

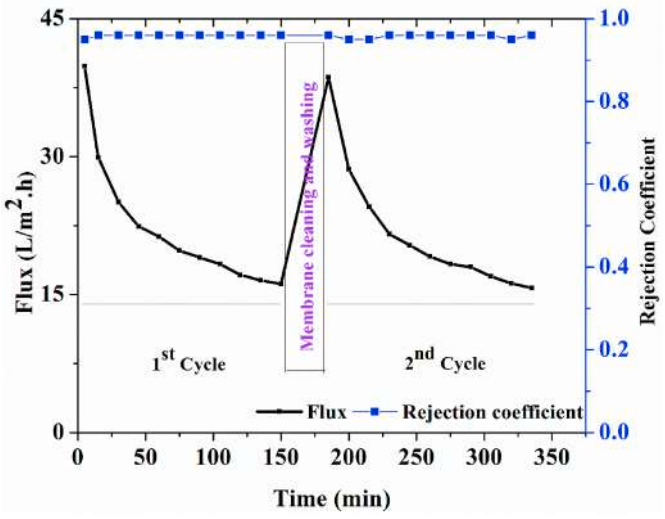

Fig. 5. Industrial cheese whey wastewater filtration analysis.

higher organic load compared to the latter. The Hermia model displayed that the flux values were a good fit within the cake layer fouling model, with a cake layer coefficient value of 4.79×10^6 s/m^2. Water recovery of up to 55% was attained within the filtration period of 150 min under low TMP of 250 kPa. This study indicates that cross-flow filtration mode at the optimum operating condition would be an effective and economically feasible method to recover whey protein from cheese whey effluent. Overall, this fouling analysis of whey solution provides an insight on the effect of different input variables to minimize fouling while enhancing flux performances. This study also provides a scope on cost effective methods for whey wastewater management.

3.4. Scope and perspectives of CNN modeling on whey wastewater filtration

Low molecular weight cutoff (PES 30 kDa) UF membrane coupled with ML showed promising advances in recovering high-value added total whey protein from cheese whey wastewater. Membrane fouling is an inherent issue while processing whey wastewater, owing to its high organic load. Optimizing hydrodynamic conditions has the potential to influence and improve UF performance in terms of flux and value-added whey recovery. Membrane fouling was significantly reduced when the input variables conditions such as pH, TMP and cross-flow velocity were optimized. Such optimizations can also help in design of cost-effective membrane modules for whey downstream processes which can be easily scaled up in the future when necessary. The proposed deep learning CNN modeling would also aid in the development of membrane integrated dairy intensification process for sustainable recovery of whey from the wastewater generated. CNN modeling could also be applied in online sensors to provide operational instruction to modules in regards to periodic washing and membrane cleaning. Physiological model was able to further shed light of the fouling mechanisms in synthetic and real time cheese whey effluent. Frugal dataset modeling using other deep learning and hybrid modeling tools can also be studied upon for process optimization within UF. Similar approaches could be extended to recover macromolecular bio-active compounds from waste streams of other food and agro-industry.

4. Conclusions

Cheese whey was effectively recovered from acid casein cheese whey solution using a PES 30 kDa membrane in both dead-end and cross-flow filtration modes. The influence of process variables on membrane fouling and concentration polarization resistance were analyzed. Feed pH altered the protein structural orientation and enhanced both membrane flux and antifouling tendency. A high whey protein retention ratio of 0.97 was observed at a pH of 8. It was due to stronger electrostatic repulsion between protein and membrane surface. Flux increases with the increase of TMP and a maximum flux was observed at the pH of 6. However, at isoelectric point, whey protein adsorbed on the membrane surface reduced the flux and led to a higher fouling resistance. Among the filtration systems, cross-flow mode operation had better flux at lower TMP. Higher flux and lower fouling resistance values of 108.23 L/m^{2}h and 2.15×10^{12} m^{-1}, respectively were observed under a TMP of 250 kPa, pH of 8 and a 1.5 m/s cross-flow velocity experimental condition. Thus, the system was able to operate under low TMP facilitating longer operation duration. Moreover, CNN exhibited good correlation with the experimental membrane flux dynamics for both cross-flow and dead-end mode system. The membrane performance was also superior when using real time cheese whey effluent under the optimized conditions.

Author credits

Y. Lukka Thuyavan: Conceptualization, Coding, Investigation, Writing - original draft, V. Kirubakaran: Coding, Writing - review & editing, Visualization, G. Arthanareeswaran: Supervision, Project administration, Resources, A.F. Ismail: Supervision, Project administration, Resources, P.S. Goh: Writing - review & editing, Visualization, N. Anantharaman: Conceptualization, Writing - review & editing, M.S. Abdullah: Methodology.

Declaration of competing interest

The authors declare that they have no known competing financial interests or personal relationships that could have appeared to influence the work reported in this paper.

Appendix A. Supplementary data

Supplementary data to this article can be found online at https://doi.org/10.1016/j.jenvman.2021.113872.

References

Adi, Z., Mahlia, T.M.I., Jaafar, J., 2019. Finned spacer for efficient membrane fouling control in produced water filtration. J. Environ. Manag. 249, 109359. https://doi.org/10.1016/j.jenvman.2019.109359.

Ahmed, N., Islam, M.N., Tuba, A.S., Mahdy, M.R.C., Sujauddin, M., 2019. Solving visual pollution with deep learning: a new nexus in environmental management. J. Environ. Manag. 248, 109253. https://doi.org/10.1016/j.jenvman.2019.07.024.

Arhoun, B., Villen-Guzman, M., Gomez-Lahoz, C., Rodriguez-Maroto, J.M., Garcia-Herruzo, F., Vereda-Alonso, C., 2019. Anaerobic co-digestion of mixed sewage sludge and fruits and vegetable wholesale market waste: composition and seasonality effect. J. Water Process Eng. 31, 100848. https://doi.org/10.1016/j.jwpe.2019.100848.

Arunkumar, A., Etzel, M.R., 2015. Negatively charged tangential flow ultrafiltration membranes for whey protein concentration. J. Membr. Sci. 475, 340–348. https://doi.org/10.1016/j.memsci.2014.10.049.

Asunis, F., De Gioannis, G., Dessì, P., Isipato, M., Lens, P.N.L., Muntoni, A., Polettini, A., Pomi, R., Rossi, A., Spiga, D., 2020. The dairy biorefinery: integrating treatment processes for cheese whey valorisation. J. Environ. Manag. 276, 111240. https://doi.org/10.1016/j.jenvman.2020.111240.

Bagheri, M., Akbari, A., Mirbagheri, S.A., 2019. Advanced control of membrane fouling in filtration systems using artificial intelligence and machine learning techniques: a critical review. Process Saf. Environ. Protect. 123, 229–252. https://doi.org/10.1016/j.psep.2019.01.013.

Becht, N.O., Malik, D.J., Tarleton, E.S., 2008. Evaluation and comparison of protein ultrafiltration test results: dead-end stirred cell compared with a cross-flow system. Separ. Purif. Technol. 62, 228–239. https://doi.org/10.1016/j.seppur.2008.01.030.

Biswas, K., Banik, I., Mukhopadhyay, D., Chowdhury, T., Majumder, A., Sarkar, D., 2021. Protein recovery from wastewater by pulsating d.c electroultrafiltration: implications of fatigue in fouling layer. J. Water Process Eng. 40, 101958. https://doi.org/10.1016/j.jwpe.2021.101958.

Cavalcanti, F.M., Schmal, M., Giudici, R., Brito Alves, R.M., 2019. A catalyst selection method for hydrogen production through Water-Gas Shift Reaction using artificial neural networks. J. Environ. Manag. 237, 585–594. https://doi.org/10.1016/j.jenvman.2019.02.092.

Charalambous, P., Vyrides, I., 2021. In situ biogas upgrading and enhancement of anaerobic digestion of cheese whey by addition of scrap or powder zero-valent iron (ZVI). J. Environ. Manag. 280, 111651. https://doi.org/10.1016/j.jenvman.2020.111651.

Chen, Jialei, Huang, G., Chen, W., 2021a. Towards better flood risk management: assessing flood risk and investigating the potential mechanism based on machine learning models. J. Environ. Manag. 293, 112810. https://doi.org/10.1016/j.jenvman.2021.112810.

Chen, Junjie, Lu, W., Xue, F., 2021b. "Looking beneath the surface": a visual-physical feature hybrid approach for unattended gauging of construction waste composition. J. Environ. Manag. 286, 112233. https://doi.org/10.1016/j.jenvman.2021.112233.

Cheng, Y., He, L.-Y., Huang, X.-F., 2021. Development of a high-performance machine learning model to predict ground ozone pollution in typical cities of China. J. Environ. Manag. 299, 113670. https://doi.org/10.1016/j.jenvman.2021.113670.

Corbatón-Báguena, María-José, Silvia Álvarez-Blanco, M.-C.V.-V., 2018. Ultrafiltration of whey: membrane performance and modelling using a combined pore blocking–cake formation model. J. Chem. Technol. Biotechnol. 93, 1891–1900. https://doi.org/10.1002/jctb.5446.

Corbatón-Báguena, M.J., Álvarez-Blanco, S., Vincent-Vela, M.C., 2018. Evaluation of fouling resistances during the ultrafiltration of whey model solutions. J. Clean. Prod. 172, 358–367. https://doi.org/10.1016/j.jclepro.2017.10.149.

Das, B., Sarkar, S., Sarkar, A., Bhattacharjee, S., Bhattacharjee, C., 2016. Recovery of whey proteins and lactose from dairy waste: a step towards green waste management. Process Saf. Environ. Protect. 101, 27–33. https://doi.org/10.1016/j.psep.2015.05.006.

Farahbakhsh, J., Delnavaz, M., Vatanpour, V., 2019. Simulation and characterization of novel reverse osmosis membrane prepared by blending polypyrrole coated multiwalled carbon nanotubes for brackish water desalination and antifouling properties using artificial neural networks. J. Membr. Sci. 581, 123–138. https://doi.org/10.1016/j.memsci.2019.03.050.

Farjami, M., Vatanpour, V., Moghadassi, A., 2020. Fabrication of a new emulsion polyvinyl chloride (EPVC) nanocomposite ultrafiltration membrane modified by para-hydroxybenzoate alumoxane (PHBA) additive to improve permeability and antifouling performance. Chem. Eng. Res. Des. 153, 8–20. https://doi.org/10.1016/j.cherd.2019.10.022.

Fernández-Rodríguez, M.J., Puntano, N.F., Mancilla-Leytón, J.M., Borja, R., 2021. Batch mesophilic anaerobic co-digestion of spent goat batch mesophilic anaerobic co-digestion of spent goat straw bedding and goat cheese whey: comparison with the mono-digestion of the two sole substrates. J. Environ. Manag. 280, 111733. https://doi.org/10.1016/j.jenvman.2020.111733.

Güneş, E., Gönder, Z.B., 2021. Evaluation of the hybrid system combining electrocoagulation, nanofiltration and reverse osmosis for biologically treated textile effluent: treatment efficiency and membrane fouling. J. Environ. Manag. 294, 113042. https://doi.org/10.1016/j.jenvman.2021.113042.

Hartinger, M., Schiffer, S., Heidebrecht, H.J., Dumpler, J., Kulozik, U., 2020. Milk protein fractionation by custom-made prototypes of spiral-wound microfiltration membranes operated at extreme crossflow velocities. J. Membr. Sci. 605, 118110. https://doi.org/10.1016/j.memsci.2020.118110.

Im, S.J., Viet, N.D., Jang, A., 2021. Real-time monitoring of forward osmosis membrane fouling in wastewater reuse process performed with a deep learning model. Chemosphere 275, 130047. https://doi.org/10.1016/j.chemosphere.2021.130047.

Jawad, J., Hawari, A.H., Zaidi, S., 2020. Modeling of forward osmosis process using artificial neural networks (ANN) to predict the permeate flux. Desalination 484, 114427. https://doi.org/10.1016/j.desal.2020.114427.

Jiang, S., Zhang, Y., Zhao, F., Yu, Z., Zhou, X., Chu, H., 2018. Impact of transmembrane pressure (TMP) on membrane fouling in microalgae harvesting with a uniform shearing vibration membrane system. Algal Res 35, 613–623. https://doi.org/10.1016/j.algal.2018.10.003.

Kekre, K.M., Anvari, A., Kahn, K., Yao, Y., Ronen, A., 2021. Reactive electrically conducting membranes for phosphorus recovery from livestock wastewater effluents. J. Environ. Manag. 282, 111432. https://doi.org/10.1016/j.jenvman.2020.111432.

Kumar, A., Vashishtha, G., Gandhi, C.P., Tang, H., Xiang, J., 2021. Tacho-less sparse CNN to detect defects in rotor-bearing systems at varying speed. Eng. Appl. Artif. Intell. 104, 104401. https://doi.org/10.1016/j.engappai.2021.104401.

Lee, J., Jeong, S., Ye, Y., Chen, V., Vigneswaran, S., Leiknes, T.O., Liu, Z., 2017. Protein fouling in carbon nanotubes enhanced ultrafiltration membrane: fouling mechanism as a function of pH and ionic strength. Separ. Purif. Technol. 176, 323–334. https://doi.org/10.1016/j.seppur.2016.10.061.

Li, H., Zeng, X., Shi, W., Zhang, H., Huang, S., Zhou, R., Qin, X., 2020. Recovery and purification of potato proteins from potato starch wastewater by hollow fiber separation membrane integrated process. Innovat. Food Sci. Emerg. Technol. 63, 102380. https://doi.org/10.1016/j.ifset.2020.102380.

Li, X., Yi, X., Liu, Z., Liu, H., Chen, T., Niu, G., Yan, B., Chen, C., Huang, M., Ying, G., 2021. Application of novel hybrid deep leaning model for cleaner production in a paper industrial wastewater treatment system. J. Clean. Prod. 294, 126343. https://doi.org/10.1016/j.jclepro.2021.126343.

Luo, J., Ding, L., Qi, B., Jaffrin, M.Y., Wan, Y., 2011. A two-stage ultrafiltration and nanofiltration process for recycling dairy wastewater. Bioresour. Technol. 102, 7437–7442. https://doi.org/10.1016/j.biortech.2011.05.012.

Ma, J., Ding, Y., Cheng, J.C.P., Jiang, F., Xu, Z., 2020. Soft detection of 5-day BOD with sparse matrix in city harbor water using deep learning techniques. Water Res. 170, 115350. https://doi.org/10.1016/j.watres.2019.115350.

Macedo, A., Duarte, E., Fragoso, R., 2015. Assessment of the performance of three ultrafiltration membranes for fractionation of ovine second cheese whey. Int. Dairy J. 48, 31–37. https://doi.org/10.1016/j.idairyj.2014.12.003.

Metsämuuronen, S., Mänttäri, M., Nyström, M., 2011. Comparison of analysis methods for protein concentration and its use in UF fractionation of whey. Desalination 283, 156–164. https://doi.org/10.1016/j.desal.2011.02.012.

Meyer, P., Mayer, A., Kulozik, U., 2015. High concentration of skim milk proteins by ultrafiltration: characterisation of a dynamic membrane system with a rotating membrane in comparison with a spiral wound membrane. Int. Dairy J. 51, 75–83. https://doi.org/10.1016/j.idairyj.2015.07.010.

Miller, D.J., Kasemset, S., Paul, D.R., Freeman, B.D., 2014. Comparison of membrane fouling at constant flux and constant transmembrane pressure conditions. J. Membr. Sci. 454, 505–515. https://doi.org/10.1016/j.memsci.2013.12.027.

Miron, S.M., de Espindola, A., Dutournié, P., Ponche, A., 2021. Study of the relationship between applied transmembrane pressure and antimicrobial activity of lysozyme. Sci. Rep. 11, 12086. https://doi.org/10.1038/s41598-021-91564-x.

Nandi, B.K., Moparthi, A., Uppaluri, R., Purkait, M.K., 2010. Treatment of oily wastewater using low cost ceramic membrane: comparative assessment of pore blocking and artificial neural network models. Chem. Eng. Res. Des. 88, 881–892. https://doi.org/10.1016/j.cherd.2009.12.005.

Ng, W., Minasny, B., McBratney, A., 2020. Convolutional neural network for soil microplastic contamination screening using infrared spectroscopy. Sci. Total Environ. 702, 134723. https://doi.org/10.1016/j.scitotenv.2019.134723.

Nourbakhsh, H., Emam-Djomeh, Z., Omid, M., Mirsaeedghazi, H., Moini, S., 2014. Prediction of red plum juice permeate flux during membrane processing with ANN optimized using RSM. Comput. Electron. Agric. 102, 1–9. https://doi.org/10.1016/j.compag.2013.12.017.

Oulebsir, R., Lefkir, A., Safri, A., Bermad, A., 2020. Optimization of the energy consumption in activated sludge process using deep learning selective modeling. Biomass Bioenergy 132, 105420. https://doi.org/10.1016/j.biombioe.2019.105420.

Park, S., Baek, S.S., Pyo, J.C., Pachepsky, Y., Park, J., Cho, K.H., 2019. Deep neural networks for modeling fouling growth and flux decline during NF/RO membrane filtration. J. Membr. Sci. 587, 117164. https://doi.org/10.1016/j.memsci.2019.06.004.

Pa'Ee, K.F., Gibson, T., Marakilova, B., Jauregi, P., 2015. Production of acid whey hydrolysates applying an integrative process: effect of calcium on process performance. Process Biochem. 50, 302–310. https://doi.org/10.1016/j.procbio.2014.11.011.

Poornapushpakala, S., Dawn, S.S., Arun Govind, M., Santhosh, A., Nirmala, N., Barani, S., Nirmala, M., 2021. A novel image processing technique to evaluate biodiesel wastewater for recovery, recycle and reuse towards zero liquid discharge approach. Biocatal. Agric. Biotechnol. 31, 101874. https://doi.org/10.1016/j.bcab.2020.101874.

Rezaei, H., Ashtiani, F.Z., Fouladitajar, A., 2011. Effects of operating parameters on fouling mechanism and membrane flux in cross-flow microfiltration of whey. Desalination 274, 262–271. https://doi.org/10.1016/j.desal.2011.02.015.

Saha, S., Boro, R., Das, C., 2019. Treatment of tea industry wastewater using coagulation-spinning basket membrane ultrafiltration hybrid system. J. Environ. Manag. 244, 180–188. https://doi.org/10.1016/j.jenvman.2019.05.043.

Sánchez-Arévalo, C.M., Carbonell-Alcaina, C., Vincent-Vela, M.C., Álvarez-Blanco, S., 2021. Effect of the operating conditions on a nanofiltration process to separate low-molecular-weight phenolic compounds from the sugars present in olive mill wastewaters. Process Saf. Environ. Protect. 148, 428–436. https://doi.org/10.1016/j.psep.2020.10.002.

Shanmugaprakash, M., Sivakumar, V., 2013. Development of experimental design approach and ANN-based models for determination of Cr(VI) ions uptake rate from aqueous solution onto the solid biodiesel waste residue. Bioresour. Technol. 148, 550–559. https://doi.org/10.1016/j.biortech.2013.08.149.

Shi, S., Xu, G., 2018. Novel performance prediction model of a biofilm system treating domestic wastewater based on stacked denoising auto-encoders deep learning network. Chem. Eng. J. 347, 280–290. https://doi.org/10.1016/j.cej.2018.04.087.

Shishegaran, A., Boushehri, A.N., Ismail, A.F., 2020. Gene expression programming for process parameter optimization during ultrafiltration of surfactant wastewater using hydrophilic polyethersulfone membrane. J. Environ. Manag. 264, 110444. https://doi.org/10.1016/j.jenvman.2020.110444.

Singh, P., Chaudhury, S., Panigrahi, B.K., 2021. Hybrid MPSO-CNN: multi-level particle swarm optimized hyperparameters of convolutional neural network. Swarm Evol. Comput. 63, 100863. https://doi.org/10.1016/j.swevo.2021.100863.

Soleimani, R., Shoushtari, N.A., Mirza, B., Salahi, A., 2013. Experimental investigation, modeling and optimization of membrane separation using artificial neural network and multi-objective optimization using genetic algorithm. Chem. Eng. Res. Des. 91, 883–903. https://doi.org/10.1016/j.cherd.2012.08.004.

Srivastava, A., K, A., Nair, A., Ram, S., Agarwal, S., Ali, J., Singh, R., Garg, M.C., 2021. Response surface methodology and artificial neural network modelling for the performance evaluation of pilot-scale hybrid nanofiltration (NF) & reverse osmosis (RO) membrane system for the treatment of brackish ground water. J. Environ. Manag. 278, 111497. https://doi.org/10.1016/j.jenvman.2020.111497.

Steinhauer, T., Schwing, J., Krauß, S., Kulozik, U., 2015. Enhancement of ultrafiltration-performance and improvement of hygienic quality during the production of whey concentrates. Int. Dairy J. 45, 8–14. https://doi.org/10.1016/j.idairyj.2015.01.010.

Sundaran, S.P., Reshmi, C.R., Sagitha, P., Manaf, O., Sujith, A., 2019. Multifunctional graphene oxide loaded nanofibrous membrane for removal of dyes and coliform from water. J. Environ. Manag. 240, 494–503. https://doi.org/10.1016/j.jenvman.2019.03.105.

Taheri, E., Amin, M.M., Fatehizadeh, A., Rezakazemi, M., Aminabhavi, T.M., 2021. Artificial intelligence modeling to predict transmembrane pressure in anaerobic membrane bioreactor-sequencing batch reactor during biohydrogen production. J. Environ. Manag. 292, 112759. https://doi.org/10.1016/j.jenvman.2021.112759.

Valiño, V., San Román, M.F., Ibáñez, R., Benito, J.M., Escudero, I., Ortiz, I., 2014. Accurate determination of key surface properties that determine the efficient separation of bovine milk BSA and LF proteins. Separ. Purif. Technol. 135, 145–157. https://doi.org/10.1016/j.seppur.2014.07.051.

Vatanpour, V., Haghighat, N., 2019. Improvement of polyvinyl chloride nano fi ltration membranes by incorporation of multiwalled carbon nanotubes modified with triethylenetetramine to use in treatment of dye wastewater. J. Environ. Manag. 242, 90–97. https://doi.org/10.1016/j.jenvman.2019.04.060.

Verma, S.P., Sarkar, B., 2020. Analysis of flux decline during rhamnolipid based micellar-enhanced ultrafiltration for simultaneous removal of Cd^{+2} and crystal violet from aqueous solution. J. Water Process Eng. 33, 101048. https://doi.org/10.1016/j.jwpe.2019.101048.

Wang, K., Li, K., Zhou, L., Hu, Y., Cheng, Z., Liu, J., Chen, C., 2019. Multiple convolutional neural networks for multivariate time series prediction. Neurocomputing 360, 107–119. https://doi.org/10.1016/j.neucom.2019.05.023.

Wang, J., Du, P., Hao, Y., Ma, X., Niu, T., Yang, W., 2020. An innovative hybrid model based on outlier detection and correction algorithm and heuristic intelligent optimization algorithm for daily air quality index forecasting. J. Environ. Manag. 255, 109855. https://doi.org/10.1016/j.jenvman.2019.109855.

Wen-qiong, W., Lan-wei, Z., Xue, H., Yi, L., 2017. Cheese whey protein recovery by ultrafiltration through transglutaminase (TG) catalysis whey protein cross-linking. Food Chem. 215, 31–40. https://doi.org/10.1016/j.foodchem.2016.07.057.

Yadav, R.K., Anubhav, 2020. PSO-GA based hybrid with adam optimization for ANN training with application in medical diagnosis. Cognit. Syst. Res. 64, 191–199. https://doi.org/10.1016/j.cogsys.2020.08.011.

Yadav, J.S.S., Yan, S., Pilli, S., Kumar, L., Tyagi, R.D., Surampalli, R.Y., 2015. Cheese whey: a potential resource to transform into bioprotein, functional/nutritional proteins and bioactive peptides. Biotechnol. Adv. 33, 756–774. https://doi.org/10.1016/j.biotechadv.2015.07.002.

Yaqub, M., Asif, H., Kim, S., Lee, W., 2020. Modeling of a full-scale sewage treatment plant to predict the nutrient removal efficiency using a long short-term memory (LSTM) neural network. J. Water Process Eng. 37, 101388. https://doi.org/10.1016/j.jwpe.2020.101388.

Yogarathinam, L.T., Gangasalam, A., Ismail, A.F., Arumugam, S., Narayanan, A., 2018. Concentration of whey protein from cheese whey effluent using ultrafiltration by combination of hydrophilic metal oxides and hydrophobic polymer. J. Chem. Technol. Biotechnol. 93, 2576–2591. https://doi.org/10.1002/jctb.5611.

Yogarathinam, L.T., Velswamy, K., Gangasalam, A., Ismail, A.F., Goh, P.S., Subramaniam, M.N., Satya Narayana, M., Yaacob, N., Abdullah, M.S., 2022. Parametric analysis of lignocellulosic ultrafiltration in lab scale cross flow module using pore blocking and artificial neural network model. Chemosphere 286, 131822. https://doi.org/10.1016/j.chemosphere.2021.131822.

Zhang, Q., Li, Y., Wang, Z., Qi, B., Sui, X., Jiang, L., 2019. Recovery of high value-added protein from enzyme-assisted aqueous extraction (EAE) of soybeans by dead-end ultrafiltration. Food Sci. Nutr. 7, 858–868. https://doi.org/10.1002/fsn3.936.